Supercritical and transcritical real-fluid mixing in diesel engine applications

By P. C. Ma, L. Bravo† AND M. Ihme

A numerical framework for simulating the mixing of supercritical and transcritical fluids with large density ratios is presented. The accurate and robust modeling of real-fluid effects on the fuel/air mixing process is critical in characterizing engine combustion. To describe this mixing process, the double-flux model is extended to systems with real-fluid state equations. For this, an effective specific heat ratio is introduced to eliminate the spurious pressure oscillations that are caused by the nonlinearity of the real-fluid equation of state. High-order WENO spatial discretization scheme is used for the real-fluid flow calculations to account for the large density gradients associated with these flows. One-dimensional single and multicomponent advection test cases and two-dimensional supercritical nitrogen jet mixing and transcritical *n*-dodecane injection test cases are conducted to show the capability of the present study in application to real-fluid supercritical and transcritical flows. Energy conservation errors, generated due to the double-flux formulation, are acceptable.

1. Introduction

A simple thermodynamic analysis inside a diesel engine combustion chamber will show that higher chamber pressures will result in higher energy output as well as higher engine efficiency. Similar trends are also found in other applications such as rocket propulsion systems and gas turbine engines. This has motivated substantial research interests in high-pressure combustion systems. When the temperature and pressure exceed their critical values, the thermodynamic state is called a supercritical state. In diesel engines, typically a subcritical liquid fuel is injected into a supercritical ambient gas and the fuel jet will be heated to a supercritical temperature before combustion. This process is often referred to as a transcritical injection. At elevated pressure, the mixture properties exhibit liquid-like densities and gas-like diffusivities, and the surface tension and enthalpy of vaporization approach zero (Yang 2000). This phenomenon has been shown by recent experimental works (Mayer *et al.* 2000; Oschwald *et al.* 2006; Chehroudi 2012). Recent research by Dahms & Oefelein (2013) also provided conceptual insights into diesel injection transition processes at high pressures. However, these complex processes are still not well understood either experimentally or numerically. Therefore, to provide insight into the high-pressure combustion systems, accurate and robust simulation tools are required for the characterization of supercritical and transcritical flows where large density gradients and thermodynamic anomalies occur.

Several difficulties require consideration for the modeling of supercritical fluid mixing numerical simulations. One of them is the large density gradients caused by the liquid-like density in the dense fluid region and the gas-like density in the supercritical ambient gas region. A typical treatment in the literature is to introduce artificial dissipation locally

† Spray Combustion Research Lab, U.S. Army Research Laboratory

where large density gradients occur (Selle & Schmitt 2010; Ruiz 2012; Terashima & Koshi 2012). Our previous work (Hickey *et al.* 2013; Hickey & Ihme 2013) implemented a hybrid central-ENO scheme analogous to shock-capturing schemes to locally switch to second-order Essentially-Non-Oscillatory (ENO) scheme in order to stabilize regions of large density gradients.

Another obstacle is spurious pressure oscillations that are generated when a fully conservative scheme is adopted, due to the high nonlinearity of the real-fluid equation of state (RF-EoS), which is similar to that of multicomponent compressible ideal gas flow calculations (Abgrall & Karni 2001). To prevent this, Ruiz (2012) derived a quasi-conservative scheme by relating the artificial dissipation terms in the mass, momentum, and energy conservation equations and setting the pressure differential to zero. Terashima & Koshi (2012) solved the pressure equation instead of the energy equation based on the work of Abgrall (1996). For ideal gas, Johnsen & Ham (2012) adopted a scheme in which an auxiliary advection equation for the specific heat ratio was solved. Although this method is suitable for well-defined interfacial flows with inert species, it is not applicable for thermodynamically complex supercritical flows in which the thermodynamic properties are dependent on temperature and species compositions. Another approach was proposed by Abgrall & Karni (2001) and Billet & Abgrall (2003) and later extended by Houim & Kuo (2011). This method is referred to as the double-flux model for ideal gas flows. However, the double-flux model has so far not been extended to RF-EoS.

In this study, we propose a numerical scheme for the simulation of real fluids mixing at supercritical and transcritical conditions. To this end, the double-flux model is extended to the real-fluid conditions by introducing the effective specific heat ratio. High-order accurate spatial discretization, a Weighted-ENO (WENO) scheme (Jiang & Shu 1996), and the corresponding Riemann solver are applied in the real-fluid context to deal with large density gradients. Several test cases in one and two dimensions are conducted to demonstrate the capability of this scheme to deal with complex thermodynamics while maintaining robustness and high-order accuracy.

2. Mathematical formulation

2.1. *Governing equations and equation of state*

The multi-component non-reacting Navier-Stokes equation in fully conservative form is the working set of equations in the current study. A RF-EoS is adopted to account for the consistent thermodynamics in supercritical and transcritical regimes. For numerical efficiency, the state equation should be simple enough to allow for a rapid computation of the thermodynamic states while simultaneously accounting for the full complexity of the nonlinear relationship among all state quantities. The cubic Peng-Robinson equation of state (Peng & Robinson 1976) was chosen because it provides a computationally efficient and accurate state representation near the critical point (Miller *et al.* 2001). The cubic state equation is written as

$$p = \frac{\mathcal{R}T}{\mathcal{V} - \mathcal{B}_m} - \frac{\mathcal{A}_m}{\mathcal{V}^2 + 2\mathcal{V}\mathcal{B}_m + \mathcal{B}_m^2}\,, \tag{2.1}$$

where $\mathcal{V}$ and $\mathcal{R}$ represent, respectively, the molar volume and universal gas constant. The coefficients $\mathcal{A}_m$ and $\mathcal{B}_m$ are evaluated using the critical properties and temperature of the fluid. Although these equations were developed for pure fluids, mixing rules are applied to treat multi-species mixtures. A comparison of the Peng-Robinson and Soave-

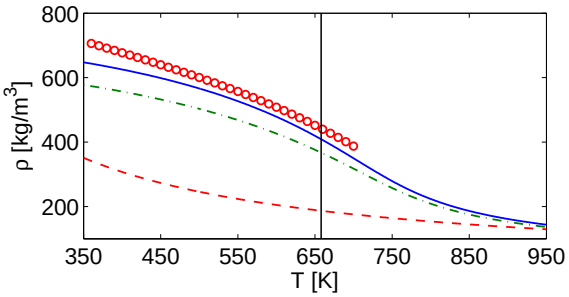

FIGURE 1. Density of *n*-dodecane at 6 MPa predicted by Peng-Robinson (——) and Soave-Redlich-Kwong (—·—) equations of state agains a NIST database (○) and ideal gas law (– – –). The vertical line shows the critical temperature of *n*-dodecane ($T_c = 658.2\,\mathrm{K}$). The critical pressure of *n*-dodecane $p_c = 1.80\,\mathrm{MPa}$.

Redlich-Kwong (Soave 1972) equations of state against NIST database for *n*-dodecane under the Spray A conditions (Pickett & Bruneaux 2011) is presented in Figure 1. The method by Chung *et al.* (1988) is used to evaluate the dynamic viscosity of the mixture. Details on the mixing rules and transport models can be found in Poling *et al.* (2001).

2.2. *Double-flux model*

To prevent spurious pressure oscillations, the double-flux model is extended to real-fluid simulations. The double-flux model was proposed by Abgrall & Karni (2001), for the computations of compressible multicomponent flows. Analysis on the Euler system shows that when a fully conservative scheme is adopted for multicomponent calorically perfect gas, the pressure equilibrium is not preserved and spurious oscillations occur. The occurrence of these instabilities is attributed to the different values of the specific heat ratio, γ, because for calorically perfect gas, the coupling between total energy and pressure is,

$$E = \rho e + \frac{1}{2}\rho u_i u_i = \frac{p}{\gamma - 1} + \frac{1}{2}\rho u_i u_i \,, \tag{2.2}$$

where E and e are total energy and specific internal energy, respectively. For multicomponent cases, γ is a nonlinear function of gas compositions. Note that for the single component calorically perfect systems, in which γ remains constant, no pressure oscillation are observed from the linear property of Eq. (2.2).

The simple single-fluid method proposed by Abgrall & Karni (2001) assumes that adjacent cells have the same γ value as that of the cell itself, when computing the flux. Note that by fixing γ the scheme is no longer fully conservative. Energy conservation errors are expected. Abgrall & Karni (2001) show that this error is proportional to the difference in γ and converges with increasing resolution. In combustion applications or supercritical jet mixing cases, the mach number is typically not very high so the small conservation errors are not expected to cause a problem (Lv & Ihme 2014). The nonlinearity between the coupling of the total energy and the pressure can arise from the temperature dependent γ typically in combustion applications. Billet & Abgrall (2003) extended the original double-flux model to account for variable γ values owning to variations in both temperature and gas compositions.

For the RF-EoS, the simple relation between specific internal energy and pressure through γ is no longer valid and instead they are coupled by an integral equation. For

Case	Pressure	$0.25\,\mathrm{m} < x < 0.75\,\mathrm{m}$	$x < 0.25\,\mathrm{m}$ or $x > 0.75\,\mathrm{m}$	Density ratio
A	4 MPa	N_2, 440.0 kg/m^3, 126.9 K	N_2, 44.5 kg/m^3, 300 K	10
B	5 MPa	H_2, 25.8 kg/m^3, 52.8 K	N_2, 50.8 kg/m^3, 332.2 K	2
C	6 MPa	*n*-dodecane, 642.0 kg/m^3, 363 K	N_2, 22.1 kg/m^3, 900 K	29

TABLE 1. Initial conditions for the one-dimensional test cases. Domain length is $x \in [0, 1]$ m.

single component cases, the expression of the specific internal energy in real fluids is

$$e(T_1, \rho_1) = e_{\mathrm{ref}} + \int_{T_{\mathrm{ref}}}^{T_1} c_v^0(T) dT + \int_0^{\rho_1} \left[p - T \left(\frac{\partial p}{\partial T} \right)_\rho \right] \frac{d\rho}{\rho^2}, \tag{2.3}$$

where e_{ref} is the reference ideal gas specific internal energy value at T_{ref}, and c_v^0 is the ideal gas specific heat capacity, which is evaluated using the NASA polynomials in the current study. The last integral term in Eq. (2.3) can be evaluated analytically based on the cubic equation of state used. Note that here the specific internal energy is a function of both temperature and density, which is different from that in the ideal gas case. To extend the double-flux model to the RF-EoS, we propose a simple effective specific heat ratio, $\tilde{\gamma}$, which is defined as follows,

$$\tilde{\gamma} = 1 + \frac{p}{\rho e}. \tag{2.4}$$

This definition is derived by relating the specific internal energy and pressure through $\rho e = p/(\tilde{\gamma} - 1)$ in analogy to the formula for specific internal energy in the ideal gas case as in Eq. (2.2). Through this effective specific heat ratio, similar procedures of the double-flux model can be applied ensuring that the pressure equilibrium will be preserved as shown in the following one-dimensional test cases.

2.3. *Spatial discretization and time advancement*

A finite volume spatial discretization scheme is adopted in the current study. A WENO reconstruction scheme was used to evaluate the left and right state values for the Riemann solver. This provides high-order accuracy and essentially non-oscillatory behavior. Primitive variables are interpolated onto the cell faces. Other choices of interpolation variables are also possible, such as conservative variables and characteristic variables that will be evaluated in future work. The procedure for converting primitive variables to conservative variables and vice versa can be found in Hickey *et al.* (2013) and Hickey & Ihme (2013). A TVD RK3 (Gottlieb & Shu 1998) time advancement scheme is adopted in the current study.

In the current study, the HLLC approximate Riemann solver is used for the solution of the Riemann problem. Several approaches are possible to estimate the wave speeds (Batten *et al.* 1997), and here the minimum and maximum of the left and right going characteristic wave speeds are used.

Similar to that of Houim & Kuo (2011), the procedure for time advancement from time t^n to time t^{n+1} using the double-flux model in the current study is summarized as follows: (i) Compute and store effective specific heat ratio $\tilde{\gamma}^n$ according to Eq. (2.4) for each cell. (ii) Reconstruct the face values of primitive variables based on the chosen spatial discretization scheme and construct the double-flux, based on the RF-EoS. (iii) Update conservative variables using the double-flux model and the time marching method. (iv)

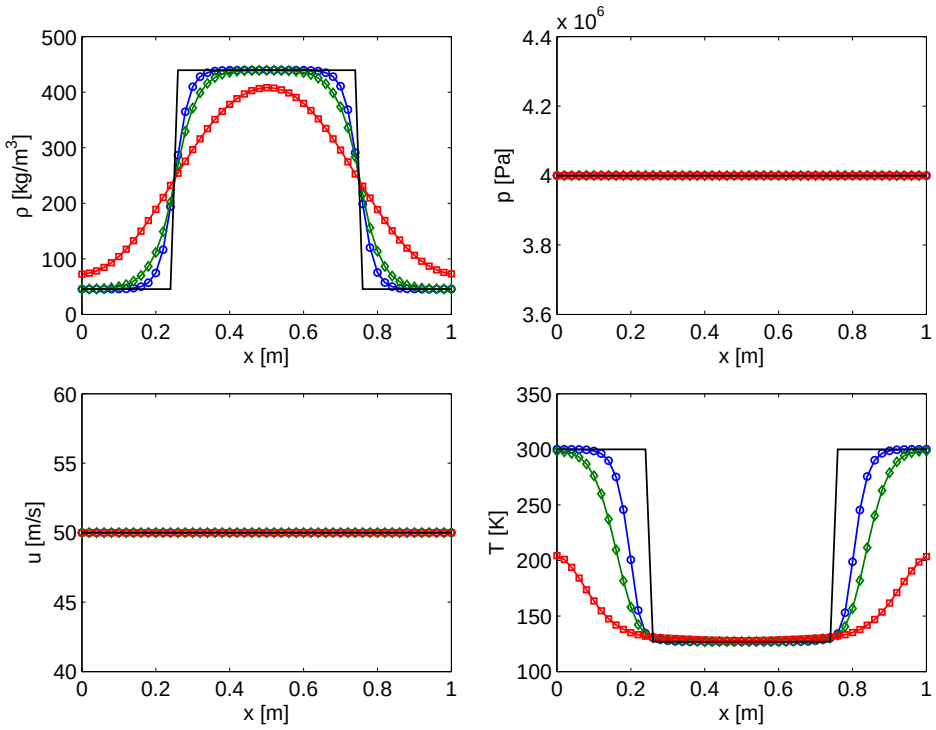

FIGURE 2. Simulation results after one period at $t = 0.02\,\mathrm{s}$ for case A. Clockwise density, pressure, velocity and temperature profiles respectively. ——, exact solution; —○—, WENO5; —◇—, WENO3; —□— , first-order upwinding.

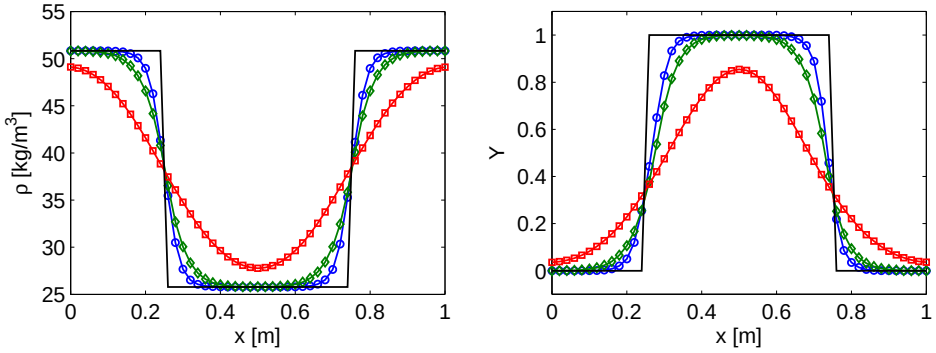

FIGURE 3. Simulation results after one period at $t = 0.02\,\mathrm{s}$ for case B. Density profile on the left and hydrogen mass fraction on the right. Same notations as in Figure 2.

Update primitive variables. For pressure, $p = (\tilde{\gamma}^n - 1)(E - \frac{1}{2}\rho u_i u_i)$. (v) Repeat steps (ii)-(iv) for each stage of the time integration scheme. (vi) After all stages of the time integration scheme are done, update conservative variables from primitive variables.

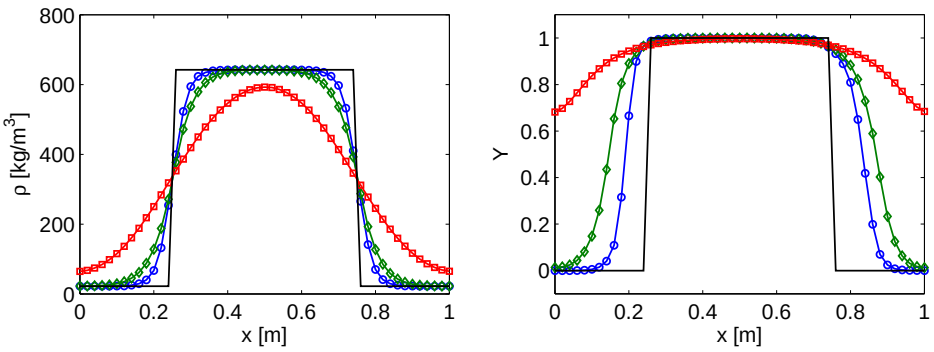

FIGURE 4. Simulation results after one period at $t = 0.02\,\mathrm{s}$ for case C. Density profile on the left and n-dodecane mass fraction on the right. Same notations as in Figure 2.

3. One-dimensional test cases

Three one-dimensional advection configurations have been selected to evaluate the performance of the proposed algorithm. Note that Euler equations are solved here, enabling a direct comparison with the analytical solutions. The initial conditions of the three test cases are listed in Table 1. The pressure for all cases is all above the critical pressure for all species considered ($p_{c,\mathrm{N_2}} = 3.40\,\mathrm{MPa}$, $p_{c,\mathrm{H_2}} = 1.28\,\mathrm{MPa}$, $p_{c,n\text{-dodecane}} = 1.80\,\mathrm{MPa}$). Case A is a supercritical case under the same conditions as the case 3 of Mayer *et al.* (2003). Cases B and C are transcritical cases, meaning that the temperature of the dense fluid is below its critical temperature ($T_{c,\mathrm{N_2}} = 126.2\,\mathrm{K}$, $T_{c,\mathrm{H_2}} = 32.9\,\mathrm{K}$, $T_{c,n\text{-dodecane}} = 658.2\,\mathrm{K}$). Case C corresponds to Spray A conditions (Pickett & Bruneaux 2011) as in diesel engine applications. The computational domain is $x \in [0, 1]$ m and for all computations 51 grid points are used, giving a uniform grid spacing of $\Delta x = 0.02\,\mathrm{m}$. Periodic boundary conditions are applied. For all computations, the CFL number is set to be 1.0. The advection velocity is 50m/s and one period is computed until $t = 0.02\,\mathrm{s}$. Three spatial discretization scheme are tested, fifth-order WENO, third-order WENO and first-order upwinding.

Figure 2 shows the results for density, pressure, velocity, and temperature profiles for case A. The present numerical scheme preserves the pressure and velocity equilibrium as expected and no spurious oscillations are generated. Note that for this cryogenic case, a fully conservative scheme will fail because of the occurrence of the spurious pressure oscillations unless an extremely large number of grid points is used to increase the spatial resolution. The density and temperature profiles do not exhibit any visible oscillations, demonstrating the capability of the WENO scheme and the HLLC Riemann solver in the context of real-fluid simulations. The first-order upwinding scheme is too diffusive in this case. The energy conservation errors are evaluated for all cases, and they remain below 1%.

Figures 3 and 4 show the results for density and mass fraction profiles for cases B and C. These two cases demonstrate the capability of the newly developed scheme for application to multicomponent real-fluid flows. No spurious oscillations of pressure or velocity are generated (results not shown here). And the density and mass fraction profiles do not show any visible fluctuations. The behavior of different spatial discretization schemes is similar to that for case A.

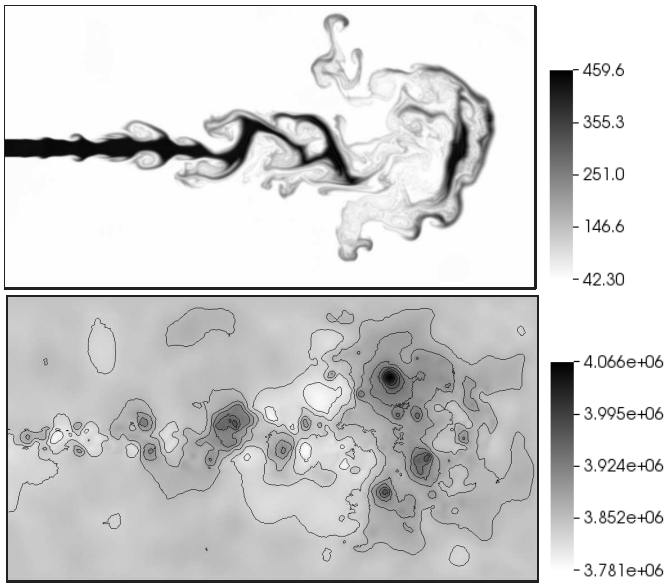

FIGURE 5. Simulation results of the planar cryogenic nitrogen jet mixing case at $t = 7.90\times10^{-4}$ s. Density profile at top (in kg/m^3) and pressure profile at bottom (in Pa). Contour ranges not adjusted. Results in full computation domain ($30h \times 16h$ where $h = 1$ mm) are shown.

4. Two-dimensional test cases

4.1. *Cryogenic nitrogen jet mixing case*

A two-dimensional cryogenic planar jet mixing case is carried out to demonstrate the multidimensional capability of the current numerical scheme. A cryogenic nitrogen jet (126.9 K) is injected into a high temperature (300 K) nitrogen vessel. The ambient pressure is initially set to be constant at 4 MPa. This case is a supercritical mixing case and similar to the condition of the case A (see Table 1) and case 3 of Mayer *et al.* (2003). Note that here the Navier-Stokes equations are solved including the viscous terms. The height of the jet exit nozzle is 1.0 mm and the jet velocity is set to be 50 m/s. A domain of $30h \times 16h$ is used, where h is the jet height. A uniform mesh in both directions is used, which has a minimum spacing of $0.04h$. The inlet condition of the jet is a plug flow with a top-hat velocity profile. Pressure outlet boundary conditions are applied at the top, bottom, and right boundaries. Adiabatic wall is applied to the left wall. No subgrid scale model is used in this case. Note that the mesh resolution is not sufficient to resolve all scales in this flow, because the purpose of this test case is to demonstrate the current numerical scheme. The solver used for the two-dimensional cases is an in-house, unstructured, finite-volume code, CharLES^x, in which the double-flux model is implemented. A hybrid central-ENO spatial discretization scheme is adopted here. The density-based sensor switches between a second-order ENO and a fourth-order central scheme to suppress spurious oscillations generated by large density gradients. Details can be found in Hickey *et al.* (2013) and Hickey & Ihme (2013).

Figure 5 shows the density and pressure fields of the nitrogen jet mixing case. The pressure field does not show any spurious oscillations in this viscous case. Note that for the viscous case, the pressure equilibrium from the Euler system is not expected. For fully conservative schemes, as used by Hickey *et al.* (2013) and Hickey & Ihme (2013),

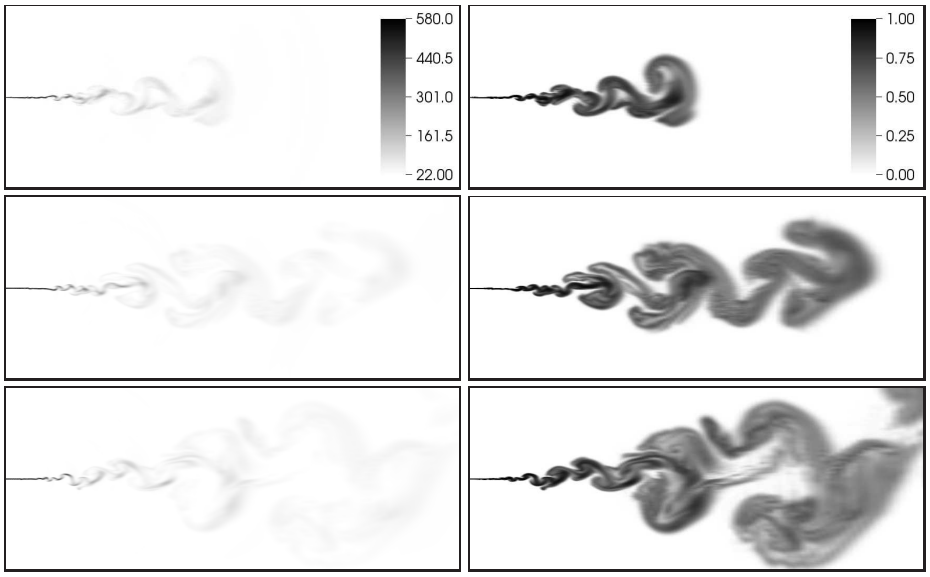

FIGURE 6. Simulation results of the transcritical *n*-dodecane injection case at time 60 µs, 120 µs and 180 µs respectively from top to bottom. Left column shows density fields (in kg/m^3) and right column shows *n*-dodecane mass fraction fields. Only portion of the computation domain ($[0, 40] \times [-8, 8]$ mm) is shown.

very fine mesh and more diffusive schemes are needed to suppress spurious oscillations. In contrast, the present scheme provides stable solutions for pressure despite the coarse mesh.

4.2. *Transcritical n-dodecane injection case*

With the success of the cryogenic nitrogen mixing case, the present numerical scheme is then tested at conditions that are more representative for diesel engine applications. For this, the injection of *n*-dodecane at 500 K into a vessel of nitrogen at 900 K is considered. The pressure is initially set to be a constant at 6 Mpa. The condition is similar to the Spray A condition (Pickett & Bruneaux 2011). Adiabatic wall boundary conditions are applied to the left, top, and bottom walls. The pressure outlet is applied at the right outlet. Plug flow is applied at the inlet. The injection velocity is set to be 650 m/s based on the mass flow rate measurements. Navier-Stokes equations are solved in the CharLES^x solver with the hybrid central-ENO scheme and the two-dimension computational domain of $800h \times 400h$ (with $h = 0.09$ mm being the injector height) is used to eliminate boundary effects. The minimum mesh spacing is 4.5 µm and total number of grid points is about 0.2 million. No subgrid scale model is applied, because the purpose of this test case is not to resolve all scales in the flow but to demonstrate the capability of the current scheme to diesel engine applications.

Figure 6 shows simulation results for density and *n*-dodecane mass fraction. During the simulation, no spurious pressure oscillations were generated. Substantially high resolution is needed for a fully conservative scheme to simulate similar conditions without significant pressure oscillations. Temperature spikes were observed in the simulation results (not shown here), and may be solved by interpolating the characteristic variable for the reconstruction (Houim & Kuo 2011). This will be addressed as a part of the future work. We have demonstrated the overall performance of the herein developed numerical

scheme by considering one- and two-dimensional test cases involving density ratio in excess of 25 and the extension to three-dimensional configurations is the focus of future work.

5. Conclusions

A numerical framework for simulating supercritical and transcritical fluid mixing with large density ratios is presented. The double-flux model is extended to RF-EoS by introducing an effective specific heat ratio to eliminate spurious pressure oscillations that are caused by the highly nonlinear RF-EoS. A high-order WENO spatial discretization scheme is used along with a TVD RK3 time integration scheme to account for large density gradients associated with these flows. One-dimensional advection test cases demonstrate the superior performance of the present numerical scheme over fully conservative schemes. The conservation errors generated by the double-flux formulation are acceptable. No spurious pressure oscillations are observed for all three test cases and no oscillations in the density field are observed. Two-dimensional test cases of supercritical nitrogen jet mixing and the transcritical *n*-dodecane injection show the capability of the present study to multidimensional flows. No spurious pressure oscillations are observed even on relatively coarse meshes. Future work includes the application of the method to three-dimensional configurations and the validation against experimental measurements.

Acknowledgments

Financial support through NSF/DOE with grant number CBET 1258609 and NASA with award numbers NNX14CM43P and NNM13AA11G are gratefully acknowledged. This study was supported in part by an appointment (LB) to the U.S. Army Research Laboratory Postdoctoral Fellowship Program administered by the Oak Ridge Associated Universities through a contract with ARL.

REFERENCES

Abgrall, R. 1996 How to prevent pressure oscillations in multicomponent flow calculations: A quasi conservative approach. *J. Comput. Phys.* **125**, 150–160.

Abgrall, R. & Karni, S. 2001 Computations of compressible multifluids. *J. Comput. Phys.* **169**, 594–623.

Batten, P., Clarke, N., Lambert, C. & Causon, D. 1997 On the choice of wavespeeds for the HLLC Riemann solver. *SIAM J. Sci. Comput.* **18**, 1553–1570.

Billet, G. & Abgrall, R. 2003 An adaptive shock-capturing algorithm for solving unsteady reactive flows. *Comput. Fluids* **32**, 1473–1495.

Chehroudi, B. 2012 Recent experimental efforts on high-pressure supercritical injection for liquid rockets and their implications. *Int. J. Aerosp. Eng.* **2012**.

Chung, T. H., Ajlan, M., Lee, L. L. & Starling, K. E. 1988 Generalized multiparameter correlation for nonpolar and polar fluid transport properties. *Ind. Eng. Chem. Res.* **27**, 671–679.

Dahms, R. N. & Oefelein, J. C. 2013 On the transition between two-phase and single-phase interface dynamics in multicomponent fluids at supercritical pressures. *Phys. Fluids.* **25**, 092103.

Gottlieb, S. & Shu, C.-W. 1998 Total variation diminishing runge-kutta schemes. *Math. Comp.* **67**, 73–85.

Hickey, J.-P. & Ihme, M. 2013 Supercritical mixing and combustion in rocket propulsion. *Annual Research Briefs*, Center for Turbulence Research, Stanford University, pp. 21–36.

Hickey, J.-P., Ma, P. C., Ihme, M. & Thakur, S. 2013 Large eddy simulation of shear coaxial rocket injector: Real fluid effects. In *AIAA Joint Propulsion Conference (AIAA 2013-4071)*.

Houim, R. W. & Kuo, K. K. 2011 A low-dissipation and time-accurate method for compressible multi-component flow with variable specific heat ratios. *J. Comput. Phys.* **230**, 8527–8553.

Jiang, G.-S. & Shu, C.-W. 1996 Efficient implementation of weighted ENO schemes. *J. Comput. Phys.* **126**, 202–228.

Johnsen, E. & Ham, F. 2012 Preventing numerical errors generated by interface-capturing schemes in compressible multi-material flows. *J. Comput. Phys.* **231**, 5705–5717.

Lv, Y. & Ihme, M. 2014 Discontinuous galerkin method for multicomponent chemically reacting flows and combustion. *J. Comput. Phys.* **270**, 105–137.

Mayer, W., Schik, A., Schaffler, M. & Tamura, H. 2000 Injection and mixing processes in high-pressure liquid oxygen/gaseous hydrogen rocket combustors. *J. Propul. Power* **16**, 823–828.

Mayer, W., Telaar, J., Branam, R., Schneider, G. & Hussong, J. 2003 Raman measurements of cryogenic injection at supercritical pressure. *Heat Mass Transfer.* **39**, 709–719.

Miller, R. S., Harstad, K. G. & Bellan, J. 2001 Direct numerical simulations of supercritical fluid mixing layers applied to heptane–nitrogen. *J. Fluid Mech.* **436**, 1–39.

Oschwald, M., Smith, J., Branam, R., Hussong, J., Schik, A., Chehroudi, B. & Talley, D. 2006 Injection of fluids into supercritical environments. *Combust. Sci. Technol.* **178**, 49–100.

Peng, D.-Y. & Robinson, D. B. 1976 A new two-constant equation of state. *Ind. Eng. Chem. Res.* **15**, 59–64.

Pickett, L. & Bruneaux, G. 2011 Engine combustion network. *Combustion Research Facility, Sandia National Laboratories, Livermore, CA. (http://www.sandia.gov/ECN)*.

Poling, B. E., Prausnitz, J. M. & O'Connell, J. P. 2001 *The Properties of Gases and Liquids*. McGraw-Hill.

Ruiz, A. 2012 *Unsteady numerical simulations of transcritical turbulent combustion in liquid rocket engines.* PhD thesis, Institut Nationale Polytechnique de Toulouse.

Selle, L. & Schmitt, T. 2010 Large-eddy simulation of single-species flows under supercritical thermodynamic conditions. *Combust. Sci. Technol.* **182**, 392–404.

Soave, G. 1972 Equilibrium constants from a modified Redlich-Kwong equation of state. *Chem. Eng. Sci.* **27**, 1197–1203.

Terashima, H. & Koshi, M. 2012 Approach for simulating gas–liquid-like flows under supercritical pressures using a high-order central differencing scheme. *J. Comput. Phys.* **231**, 6907–6923.

Yang, V. 2000 Modeling of supercritical vaporization, mixing, and combustion processes in liquid-fueled propulsion systems. *Proc. Combust. Inst.* **28**, 925–942.